HAL

archives-ouvertes.fr

On the potential of ultrasound elastography for pressure ulcer early detection.

Jean-François Deprez, Elisabeth Brusseau, Jérémie Fromageau, Guy Cloutier, Olivier Basset

On the potential of ultrasound elastography for pressure ulcer early detection

Jean-François Deprez[a] and Elisabeth Brusseau
*CREATIS Laboratory, Université de Lyon, Insa de Lyon, Université Lyon 1, CNRS UMR5220,
Inserm U1044, Villeurbanne 69621, France*

Jérémie Fromageau and Guy Cloutier
*Laboratory of Biorheology and Medical Ultrasonics, University of Montreal Hospital Research Center
(CRCHUM), Montreal, Québec H2L 2W5, Canada*

Olivier Basset
*CREATIS Laboratory, Université de Lyon, Insa de Lyon, Université Lyon 1, CNRS UMR5220,
Inserm U1044, Villeurbanne 69621, France*

Purpose: Pressure ulcers are areas of soft tissue breakdown induced by a sustained mechanical stress that damages the skin and underlying tissues. They represent a considerable burden to the society in terms of health care and cost. Yet, techniques for prevention and detection of pressure ulcers still remain very limited. In this article, the authors investigated the potential of ultrasound elastography for pressure ulcer early detection. Elastography is an imaging technique providing local information on biological tissue mechanical properties. It is relevant for pressure ulcer detection as this pathology is associated with a gradual stiffening of damaged tissues, beginning in the deeper tissues and progressing toward the skin surface.
Methods: A 2D ultrasound elastography method was proposed and its ability in terms of pressure ulcer detection was validated through numerical simulations and physical acquisitions on pressure ulcer mimicking phantoms. *In vivo* experiments on a rat model are also reported. A maintained pressure was applied on the animal thigh, with a view to generate a pressure ulcer, and ultrasound data were acquired and processed before and after application of this pressure.
Results: Numerical simulations demonstrated that a pressure ulcer can theoretically be detected at a very early stage with ultrasound elastography. Even when the ulcer region was characterized by a low stiffening (ratio of 1.8 relative to normal tissues), the corresponding elastogram clearly underlined the pathological area. This observation was confirmed by the results obtained on a physical phantom mimicking a pressure ulcer at an early stage. Computed elastograms showed strain differences between areas mimicking healthy and pathological tissues. Results corresponding to *in vivo* experiments revealed a difference in the way tissues behaved before and after the pressure was applied on the animal thigh, which strongly suggests the presence of a pathological area.
Conclusions: Experiments demonstrated that ultrasound elastography is a promising technique for pressure ulcer detection, especially at an early stage of the pathology, when the disease is still visually undetectable. In the absence of any gold standard method, this is also a first step toward the development of a quantitative technique. © *2011 American Association of Physicists in Medicine*.
[DOI: 10.1118/1.3560421]

I. INTRODUCTION

Pressure ulcers, or bedsores, are areas of soft tissue breakdown induced by a sustained mechanical stress that damages the skin and underlying tissues. They often appear after a prolonged period of immobility, during which biological tissues undergo a maintained pressure from a support (generally a bed or a wheelchair). Pressure ulcers mostly affect people with sensitivity loss or limited mobility, who are unable to feel and/or release the pressure. Elderly people, patients in hospital recovery and persons with spinal cord injury are especially at risk.

Few statistics are available to estimate the extent of this pathology. In 2001, wide variations were found for the prevalence of pressure ulcer in the United States:[1] 10%–18% in acute care, 2.3%–28% in long-term care, and 0%–29% in home care. In the United Kingdom, prevalence was estimated at 18% in 1993.[2] As life expectancy increases in western countries, this disease becomes a growing issue and represents a considerable burden to the society in terms of health care and associated cost.[3,4]

Despite these numbers, techniques for prevention and detection of pressure ulcer still remain very limited. For instance, risk scales do exist but they are mostly used for hospitalized patients, and their efficiency is largely questioned.[5]

65 Thus, detection and prevention are mainly based on the ex-
66 perience of the health-care personnel.

67 Different approaches were developed to study skin
68 wounds. A good review of wound measurement techniques
69 can be found in Ref. 6. These techniques can be divided into
70 two categories: Visual assessment tools, based on color and
71 digital image analysis, and physiological-based tools (i.e.,
72 blood flow, force, or pressure measurements). More recently,
73 Weber *et al.*[7] developed a device to map the electrical im-
74 pedance of a wound in order to determine the wound sever-
75 ity. Treuillet *et al.*[8] also presented an original approach to
76 build 3D models of skin wounds from digital camera snap-
77 shots, allowing quantitative measurements of the wound,
78 such as surface, depth, or volume.

79 Attempts to develop quantitative techniques for detection
80 or prevention of pressure ulcers are far less numerous. In
81 Ref. 9, 15 pressure ulcers were examined using four different
82 noninvasive techniques: Skin temperature, redness index,
83 skin retraction time, and ultrasound (US) scanning. Results
84 showed that temperature and retraction time could not alone
85 characterize the ulceration stage, while a redness index was
86 useful in some cases. Ultrasound image processing could de-
87 tect a subepidermal layer, which may be a good indicator that
88 the skin is at risk. One can finally cite Ref. 10, where pre-
89 vention of pressure ulcer was based on both movement mea-
90 surement and autonomous nervous system analysis. Even
91 though these studies were constructive, it is still relevant to
92 develop new quantitative approaches.

93 This lack of quantitative assessment tools is likely the
94 result of a limited understanding of the pathology itself.
95 There is indeed very little literature on the process that trig-
96 gers the formation of pressure ulcers.

97 To date, the most established theory is that tissue com-
98 pression locally results in the occlusion of blood
99 capillaries.[11–13] The mechanism leading to the formation of a
100 pressure ulcer is linked with a shortage of blood supply,
101 called ischemia, which prevents the natural exchanges of
102 oxygen and nutrients. If the microcirculatory flow distur-
103 bance remains for too long, the ischemic condition leads to
104 cell death and tissue damages.

105 It is also acknowledged that pressure ulcers are associated
106 with a stiffening of damaged tissues, as shown in Refs. 14
107 and 15 on a rat model and on a realistic numerical model of
108 human buttocks, respectively.

109 Finally, recent studies suggest that pressure ulcers can
110 form either superficially or within deep tissues.[11,16,17] Super-
111 ficial pressure ulcers arise in the skin. They are mainly
112 caused by shear stresses and are easily detected by careful
113 skin inspection. On the other hand, deep pressure ulcers (also
114 called deep tissue injuries) develop in deep muscle layers
115 covering bony prominences and are caused by sustained
116 compression of the tissues. They follow a "deep-to-
117 superficial" pattern and progress toward the skin surface.
118 Therefore, severe necrosis of subcutaneous tissues may occur
119 while the skin shows only minor signs of tissue breakdown.
120 Consequently, deep ulcers are very difficult to identify. Since
121 deep pressure ulcers are characterized by stiffening and a

122 deep-to-superficial growing process, providing information
123 on tissue local mechanical properties could be of major in-
124 terest for physicians.

125 Accordingly, US elastography is proposed for pressure ul-
126 cer early detection. US elastography[18,19] is indeed providing
127 to clinicians information on the local mechanical properties
128 of soft biological tissues. This information, generally dis-
129 played as an image, enables the detection of unexpected stiff
130 area within healthy tissues. Typical applications of US elas-
131 tography are targeted to diseases such as breast and prostate
132 cancer,[20,21] liver fibrosis,[22] and atherosclerosis.[23]

133 Potentially, pressure ulcer US elastography could be used
134 for diagnosis and wound healing follow-up. US elastography
135 also has the advantage of being noninvasive, low-cost, and
136 portable.

137 In this paper, we investigated the potential of quasistatic
138 US elastography for pressure ulcer early detection. The paper
139 is organized as follows. Section II provides a description of
140 the US elastography method, followed by its application to
141 numerical data in Sec. III, and to a pressure ulcer mimicking
142 phantom in Sec. IV. Section V is dedicated to the presenta-
143 tion of results obtained during an *in vivo* experiment. The
144 final section provides a critical discussion and concluding
145 remarks.

II. METHOD

147 Depending on the mechanical excitation applied to the
148 tissues, there are mainly two approaches in US elastography,
149 termed quasistatic elastography[19,24–26] and dynamic
150 elastography.[18,27–29] This paper falls into the category of qua-
151 sistatic elastography, which investigates tissue deformation
152 under compression. In quasistatic elastography, information
153 on tissue local mechanical properties is deduced from a
154 simple principle: Subjected to a given stress, soft areas will
155 deform more than stiffer ones. In practical terms, for a tissue
156 under investigation, two US radiofrequency (RF) data sets
157 are acquired, corresponding to two different stress levels
158 called pre- and postcompression states. Pattern changes in-
159 duced by the stress within the RF signals are then analyzed
160 to compute a map of local strains.

161 The different steps leading to this local strain estimation
162 are briefly explained hereafter to make the paper self-
163 contained. The interested reader can refer to Refs. 26 and 30
164 for more details.

II.A. Image deformation model

166 To achieve a local estimation, images were divided into
167 multiple small regions-of-interest (ROIs) and for each ROI,
168 the effects of the tissue compression were analyzed. Most of
169 the 2D techniques used in elastography model the
170 compression-induced tissue motion as a local 2D translation
171 and then compute strain as the gradient of the resulting dis-
172 placement field. Contrary to these techniques, we considered
173 that the effect of compression on each ROI can be modeled
174 as an affine transformation. In addition to a 2D translation, a
175 scaling of the ROI was also considered, which reflects more
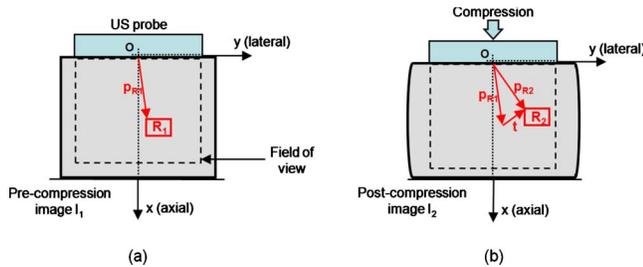**176** realistically the tissue deformation at this location.

FIG. 1. Region of interest positioning in (a) the precompression image and (b) the postcompression image.

177 However, US data resolution is highly anisotropic. Owing **178** to US device characteristics, lateral resolution is much **179** coarser than the axial resolution, which makes an accurate **180** estimation of a scaling factor difficult in the lateral direction. **181** This has led us to consider only an axial scaling of the ROI, **182** the lateral deformation being taken into account in the lateral **183** translation of the ROI.

184 II.B. ROI displacement

185 Let us denote I_1 and I_2 the pre- and postcompression im- **186** ages, respectively. Let us consider R_1 a ROI of dimensions **187** $L_{x1} \times L_{y1}$, located at p_{R1} in I_1. Finally, let us denote R_2 the **188** ROI in I_2 corresponding to the same tissue region after de- **189** formation. Its axial and lateral dimensions L_{x2} and L_{y2} are **190** such that $L_{x2} = \alpha \cdot L_{x1}$ (axial scaling) and $L_{y2} = L_{y1}$. The posi- **191** tion of R_2 in I_2, namely, p_{R2}, is also different from p_{R1}, as **192** shown in Fig. 1. We therefore initialize R_2 at its most prob- **193** able position in I_2 as

194 $$p_{R2\text{ini}} = p_{R1} + t, \qquad (1)$$

195 with $t(t_{\text{ax}}, t_{\text{lat}})$ a 2D translation. This translation vector repre- **196** sents the effects of tissue deformation on the position of R_2. **197** In particular, its axial component t_{ax} results from the axial **198** scaling of the regions located between the probe and the ROI **199** currently considered. It can therefore be entirely determined **200** from previous computations by beginning the estimation pro- **201** cess for the regions at the interface with the probe (where **202** $t_{\text{ax}} = 0$) and propagating this process to regions downward. **203** Similarly, the lateral shift t_{lat} is directly given by the previous **204** estimations, by beginning the estimation process for the re- **205** gions at the center of the probe and propagating this process **206** to the lateral sides.

207 II.C. Problem formulation

208 For the positions of R_1 and R_2 that have been determined, **209** two local parameters must now be estimated: An axial scal- **210** ing α and a residual lateral shift τ. This estimation is per- **211** formed through the minimization of an objective function f, **212** which is defined as the opposite of the normalized correla- **213** tion coefficient between R_1 and R_2, R_2 varying with these **214** parameters.

215 Since RF US data are oscillating signals by nature, the **216** function f may exhibit several local minima. To narrow the **217** optimization process around the area corresponding to the

218 global minimum, the range of values allowed for the param- **219** eters is reduced. This reduction in the parameter domain is **220** reasonable since in elastography, deformations induced by **221** the external load are of small magnitude (a few %). R_2 is **222** therefore sought in a small region immediately surrounding **223** its initial position. As a result, the optimization is subjected **224** to a set of linear inequality constraints on the parameters and **225** the problem to be solved can be formulated as

226 $$\begin{bmatrix} \hat{\alpha} & \hat{\tau} \end{bmatrix} = \underset{\alpha, \tau}{\arg \min} \, f(\alpha, \tau) \quad \text{with} \quad \begin{cases} \alpha_{\min} \leq \alpha \leq \alpha_{\max} \\ \tau_{\min} \leq \tau \leq \tau_{\max} \end{cases}. \qquad (2)$$

227 Typically, axial strain is restricted to the range $[0\%-6\%]$ and **228** lateral shift is limited to three times the RF line interspacing **229** (i.e., $\alpha_{\min} = 0.94$, $\alpha_{\max} = 1$, $\tau_{\min} = -3$, and $\tau_{\max} = 3$).

230 In practical terms, this optimization process is imple- **231** mented, thanks to a sequential quadratic programming **232** methodology,[31] together with an active set strategy. To en- **233** sure a reliable estimation and prevent the objective function **234** from being trapped in a local minimum, correction proce- **235** dures are also considered based on multiple initializations of **236** the process[26,30]

II.D. Axial strain computation   **237**

238 In this paper, the mechanical parameter we are interested **239** in is the medium's axial strain. This information is directly **240** deduced from the estimated axial scaling factor $\hat{\alpha}$, according **241** to the following relation:

242 $$\varepsilon = \hat{\alpha} - 1. \qquad (3)$$

243 It should be stressed that with Eq. (3), strain is negative for a **244** compression and positive for a dilatation. Because in this **245** study, all experiments were performed by applying a com- **246** pression to the observed media, computed strain values were **247** negative. For simplification purposes, we chose to display **248** the opposite of the strain, leading to elastograms with posi- **249** tive values, keeping in mind that they represent the percent- **250** age of medium compression.

III. NUMERICAL SIMULATIONS   **251**

252 Deep pressure ulcers develop at the deepest level and pro- **253** ceeds outward until they reach the skin.[11,16,17] At an early **254** stage of the pathology, deep tissues are therefore damaged **255** while the epidermis is still intact. Besides, areas particularly **256** exposed to pressure ulcers are those over bony prominences, **257** such as the sacrum, hips, and heels, which represent 80% of **258** bedsores.[32] From this background, a numerical phantom of **259** pressure ulcer was designed with regard to these observa- **260** tions, and the potential of US elastography for the early de- **261** tection of this condition was investigated.

262 The phantom of $30 \times 20 \times 4$ mm^3 modeled a deep ulcer **263** at the very beginning of the pathological process (Fig. 2). It **264** was made of three different regions:

265 – Healthy soft tissues in contact with the US probe, **266** – A bony prominence at the bottom, which is a privileged **267** configuration for pressure ulcer formation,
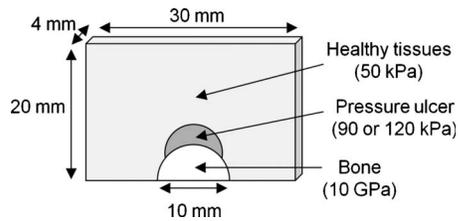
FIG. 2. Sketch of the numerical phantom mimicking a pressure ulcer at an early stage.
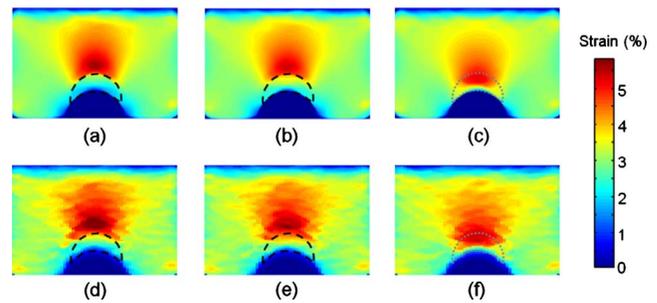

FIG. 3. Numerical phantom results. On the first row are the theoretical axial strain fields (given by the FEM) and on the second row are the estimated axial strain fields (in %). (a) and (d) are the fields for the configuration including a 120 kPa pressure ulcer. (b) and (e) are the fields for the configuration with a 90 kPa pressure ulcer. (c) and (f) are the fields for the configuration without pressure ulcer.

268 – And an intermediate layer mimicking the *in-*
269 *development* ulcer, located above the bone, and whose
270 limited size made it visually undetectable from the
271 phantom upper surface.
272 The phantom mechanical properties were defined as fol-
273 lows: The Young's modulus of the bone was set to 10 GPa
274 and that of healthy tissues was set to 50 kPa. These are
275 orders of magnitude reported in literature.[33–35] The modeling
276 of the pressure ulcer was based on the following observation.
277 During their experiments, Gefen *et al.*[14] measured a 1.8–3.3-
278 fold stiffening of tissues damaged by a pressure ulcer com-
279 pared to normal ones. Accordingly, two different values were
280 chosen for the Young's modulus of the pressure ulcer: Either
281 90 kPa, corresponding to the lowest ratio (1.8×50 kPa), or
282 120 kPa, corresponding to a middle range value. In addition,
283 a third configuration was considered for control. It repre-
284 sented a "healthy" state, with no pressure ulcer (Young's
285 modulus of 50 kPa).
286 To obtain the postcompression configuration, a 1.5 kPa
287 stress was applied on the upper surface of phantoms down-
288 ward. The corresponding tissue deformations were computed
289 through the use of a finite element modeling (FEM) package
290 (COMSOL MULTIPHYSICS, Comsol Inc., USA).
291 From an acoustical point of view, tissues were modeled as
292 a large number of punctual scatterers randomly distributed in
293 the region-of-interest. In the absence of information related
294 to pressure ulcer echogenicity and since our technique is
295 based only on tissue's stiffness differences, healthy and
296 pathological tissues were considered as having identical
297 acoustical properties. Consequently, a standard B-mode im-
298 age did not allow seeing any difference between these two
299 regions. On the other hand, the bone was designed to be
300 hyperechoic compared to soft tissues.
301 US RF data were the result of the convolution between
302 scatterers and a point spread function simulating the acous-
303 tical response of the scanner.[36] Simulations were performed
304 for both the pre- and the postcompression states, displace-
305 ments of scatterers between the two states being given by the
306 FEM.
307 The strain estimator described in Sec. II was applied to
308 these simulated data. The corresponding results, together
309 with theoretical fields, are given in Fig. 3. We can first ob-
310 serve that the estimated elastograms are close to the theoret-
311 ical fields provided by the FEM. They both exhibit similar
312 patterns of strains, which is satisfying regarding the strain
313 estimation method. The bone has a deformation close to
314 zero, which is consistent with its stiffness, and it is clearly

315 identified in the three elastograms. Its position also matches
316 the hyperechoic region of the B-mode image. Although the
317 pressure ulcer cannot be detected in the B-mode scan, the
318 presence of a hard pathological area is revealed in the elas-
319 tograms [Figs. 3(d) and 3(e)]: Strain for the pathological area
320 is indeed half that of its upper neighborhood (about 2.5% vs
321 5%). Transitions from the healthy tissues to the ulcer and
322 from the ulcer to the bone are very sharp. This underlines the
323 hard region, with limits corresponding to the dotted line
324 (area available from the FEM and added manually on the
325 different maps). In contrast, the maps corresponding to the
326 healthy model [Figs. 3(c) and 3(f)] show a relatively differ-
327 ent configuration, with a smaller maximum and the region of
328 highest strain overlapping the area of the ulcer.

IV. PRESSURE ULCER MIMICKING PHANTOM 329

330 In this section, additional tests are reported on a physical
331 phantom designed to mimic an early stage pressure ulcer. A
332 sketch of the phantom is shown in Fig. 4(a). It consisted of a
333 $30 \times 60 \times 110$ mm³ parallelepiped, within which three re-
334 gions can be identified: A bone, a region representing the
335 in-development pressure ulcer, and the surrounding healthy
336 tissues. The bone, of 10 mm in diameter, was a sample from
337 the forward limb of a dog. Other regions were made of poly-
338 vinyl alcohol (PVA) cryogel. PVA cryogel is a polymer that
339 was introduced in the 1990s to build phantoms mimicking
340 soft tissues.[37] Mixed with Sigmacell particles (Sigmacell
341 Cellulose, type 20, Sigma-Aldrich, USA), its acoustical
342 properties are close to those of soft biological tissues, and
343 this material is suitable for US imaging. Moreover, the ma-
344 terial stiffness increases with the number of freeze-thaw
345 cycles applied. By varying this number of cycles, a wide
346 range of elasticity values can be obtained, especially those
347 commonly met for soft biological tissues.[38,39] Since a pres-
348 sure ulcer is stiffer than healthy tissues, the PVA cryogel for
349 this region went through two freeze-thaw cycles, while the
350 PVA cryogel for the healthy region underwent a single cycle.
351 Such a pressure ulcer corresponds to a deep tissue injury.
352 RF US data were acquired with an *Ultrasonix Sonix RP*
353 device (Ultrasonix Medical Corporation, Richmond, BC,
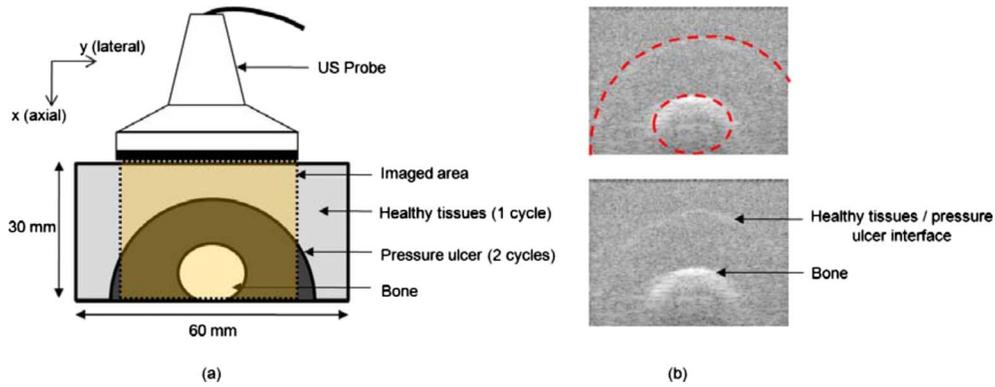354 Canada), equipped with a 7 MHz linear probe (reference

FIG. 4. (a) PVA phantom constitution. (b) B-mode image of the phantom.

355 L14-5/38). The postcompression data were acquired after
356 uniform compression of the top surface of the phantom (ap-
357 plied with a plate, while the bottom surface remained fixed).
358 These data were then processed with our strain estimator.

359   As it can be seen from the B-mode image of this region
360 [Fig. 4(b)], the bone could be clearly identified from its
361 specular reflection. However, the echography did not provide
362 any information about the mechanical properties of the phan-
363 tom. On the contrary, the estimated axial strain map (Fig. 5)
364 was helpful for the detection of the three regions of the phan-
365 tom. Even if strain values remained within a small range, it
366 can be seen that pathological tissues exhibit a different pat-
367 tern compared to the surrounding healthy soft tissues. Fi-
368 nally, deformation of the bone is almost negligible, as ex-
369 pected.

370   Mean strain were calculated for the different tissue types.
371 They were equal to $1.01 \pm 0.24\%$, $0.45 \pm 0.16\%$, and
372 $0.06 \pm 0.06\%$ for the healthy, pathological, and bone regions,
373 respectively.

V. PRELIMINARY *IN VIVO* STUDY

375   To further evaluate the contribution of elastography for
376 pressure ulcer detection, *in vivo* acquisitions on an experi-
377 mental rat model were performed. The intent of this study
378 was to investigate *in vivo* the ability of elastography to detect
379 strain, when the tissues under examination were subjected to
380 a long-term unrelieved pressure.

381   The main reason for tissue breakdown is ischemia,[11–13] in
382 connection with the interface pressure at the skin level. Tra-
383 ditionally, the value of 32 mm Hg (4.3 kPa) is quoted for the
384 pressure threshold that triggers capillary closure:[40] If main-
385 tained, interface pressures higher than this value are sup-

386 posed to lead to tissue damage. However, a more recent
387 study demonstrates that this value is not relevant since cap-
388 illary closure mainly depends on the local pressure.[41] To in-
389 duce tissue breakdown, we therefore chose to adapt the pro-
390 tocol described by Gefen *et al.*,[14] where a maintained
391 compression was applied on the thigh of rats to generate
392 pressure ulcers. In the latter paper, it is shown that a pressure
393 of 35 kPa maintained during 60 min leads to a twofold stiff-
394 ening of tissues with cell death.

395   The protocol for animal experimentation was approved by
396 the Animal Care Committee of the Centre Hospitalier de
397 l'Université de Montréal, in accordance with the guidelines
398 of the Canadian Council of Animal Care. The animal was an
399 18-week-old male rat from the Brown Norway breed and
400 weighed 265 g. It was first anesthetized by inhalation of
401 2.5% isofluorane, the hair of the hind limb was carefully
402 shaved, and the animal was then immobilized. Its body tem-
403 perature was monitored with a rectal probe (Thermalert
404 TH-5, Physitemp Instruments, Clifton, USA) and maintained
405 at 37 ± 1 °C with a heating surface. A first set of RF US data
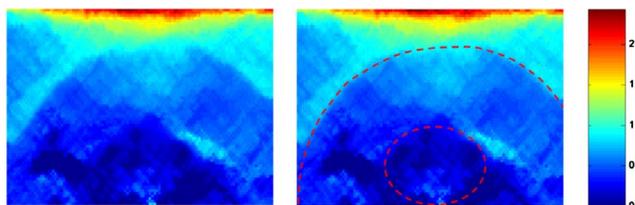

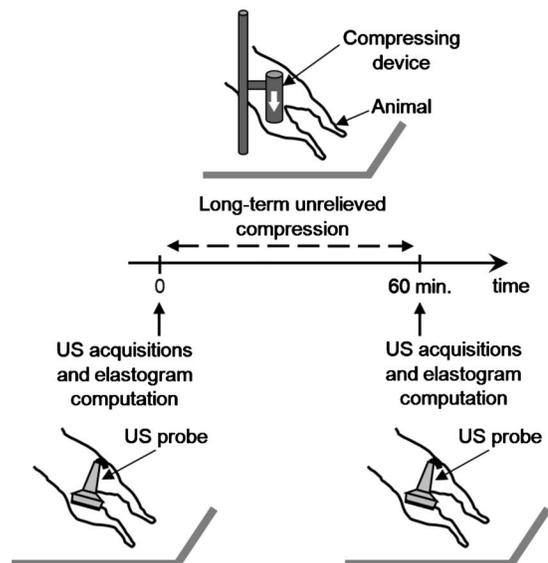FIG. 5. Estimated strain map (in %) for the PVA cryogel phantom.

FIG. 6. Scheme of the *in vivo* protocol used to induce a pressure ulcer early detection on a rat and to acquire US data for elastography imaging.
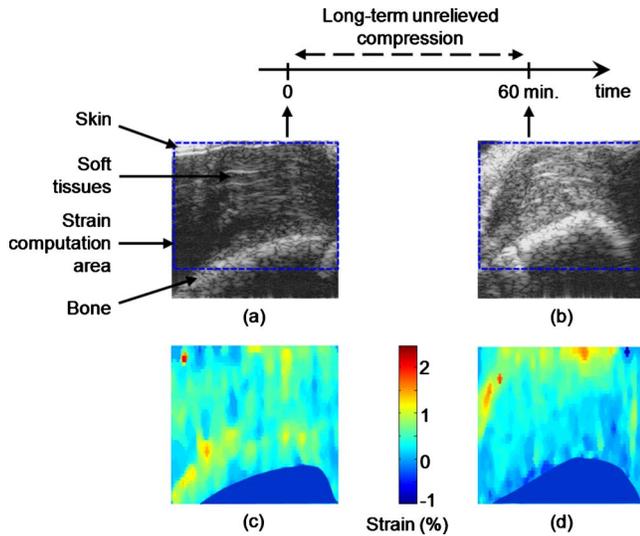
FIG. 7. B-mode images and elastograms for the *in vivo* experiment. (a) Initial B-mode image (showing the different tissues). (b) B-mode image after 60 min compression. (c) Initial elastogram. (d) Elastogram after 60 min compression.

TABLE I. Mean strain and standard deviation, according to time and location of the ROI, for the *in vivo* experiment.

Mean strain (%)		Time	
		0 min	60 min
ROI location	Close to the skin	0.48 ± 0.22	0.50 ± 0.27
	Close to the bone	0.47 ± 0.19	0.13 ± 0.13

406 was acquired, in a view to compute elastograms. A 35 kPa
407 pressure was then applied on the thigh of the animal during
408 60 min to generate a pressure ulcer. A second set of RF US
409 data was acquired after the 60 min compression. Once the
410 experiments were completed, the animal was euthanized by
411 inhalation of CO_2. Figure 6 summarizes the protocol.
412   RF US data were acquired with a *VisualSonics Vevo 660*
413 device (VisualSonics Inc., Toronto, Canada), equipped with a
414 35 MHz probe dedicated to small animal studies. US data
415 were acquired with the same settings of the scanner and were
416 processed to compute elastograms before the application of
417 the compression and after the 60 min compression. The com-
418 pression tool was a wooden stick, whose end was a 2-cm-in-
419 diameter disk in contact with the skin of the animal. Both the
420 US probe and the compression device were mounted on a
421 robotic arm (described in detail in Ref. 42). The latter was a
422 6 degrees of freedom industrial robot (F3 Articulated Robot,
423 CRS Robotics Corporation, Burlington, Canada), equipped
424 with a force sensor on its end (ATI, Industrial Automation,
425 Apex, USA), and controlled through a software interface (In-
426 tegral Technologies Inc., Laval, Canada). This enabled the
427 control of the pressure applied with the compressing device
428 and ensured an accurate positioning of the US probe.
429   Results of this experiment are presented in Fig. 7. Figure
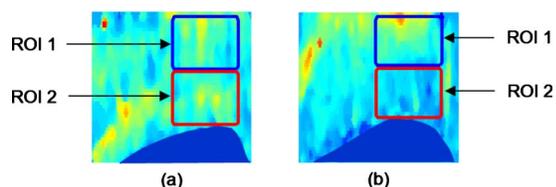**430** 7(a) provides a B-mode image of the investigated area where

431 different tissues can be identified: The skin, the bone (both
432 hyperechoic), and soft tissues, which is the region that was
433 specifically analyzed. The corresponding B-mode image af-
434 ter the application of the 60 min compression is shown in
435 Fig. 7(b). Due to the 60 min compression, the B-mode im-
436 ages exhibit different patterns. However, these images alone
437 are not relevant to reveal or not the presence of a pathologi-
438 cal area. Computed elastograms are displayed in Figs. 7(c)
439 and 7(d), respectively. The initial elastogram appears homo-
440 geneous. Only the area immediately above the bone exhibits
441 a slightly higher strain. As a comparison, the same area on
442 the second elastogram (i.e., after 60 min compression) be-
443 haved differently, with a deformation smaller than the sur-
444 rounding tissues. A sharp evolution of the strain along depth
445 is also visible for the whole image: Shallow tissues seem to
446 exhibit higher strains compared to the tissues near the bone.
447 This evolution tends to show that the tissue area over the
448 bone became stiffer, which could be the indication of an
449 emerging pressure ulcer.
450   To support this visual impression, mean deformations
451 were calculated in two ROIs, as shown in Fig. 8. For a given
452 image, both ROIs have the same size. They are also located
453 at the same lateral position, but at different depths, either
454 near the skin or near the bone. Mean strain was estimated
455 over the pixels located within the perimeter defined by the
456 ROI. The corresponding results are given in Table I. Before
457 the compression was applied ($t=0$), the strain was almost the
458 same for both regions (0.48% for the top ROI and 0.47% for
459 the bottom ROI). On the other hand, mean strains were sig-
460 nificantly different after the compression of 60 min: While
461 the mean strain for the top ROI was 0.50%, that for the
462 bottom ROI dropped to 0.13%. The large decrease in strain
463 near the bone might be due to tissue stiffening in this region.
464 This observation allows to assume that the area near the bone
465 was pathological, corresponding to the presence of a pressure
466 ulcer or, at least, corresponding to tissues that underwent a
467 degradation such that they were significantly stiffer than
468 healthy tissues.

VI. DISCUSSION AND CONCLUSION   **469**

470   In this paper, we proposed a new approach based on ul-
471 trasound imaging to address the challenging problem of pres-
472 sure ulcer early detection. Even though US elastography usu-
473 ally finds its main application in cancer tumor detection, we
474 think it has great potential for pressure ulcer early detection.
475 Since this pathology is associated with a stiffening of dam-
476 aged tissues, highlighting abnormally hard areas could in-
477 deed be fundamental. Moreover, deep pressure ulcers are

FIG. 8. Location of the ROIs for mean strain computation (a) on the initial elastogram and (b) on the final elastogram.

characterized by a deep-to-superficial pattern: The ulcer develops in deep muscle tissues and progresses toward the skin. US elastography is therefore an interesting tool for early detection, when the deep ulcer is still imperceptible by visual inspection.

To investigate the usefulness of US elastography, different types of data were processed. Numerical simulations demonstrated that a pressure ulcer can theoretically be detected at a very early stage with US elastography. Even when the ulcer region was characterized by a low stiffening (ratio of 1.8 relative to normal tissues), the estimated elastogram clearly underlined the pathological area.

This observation was confirmed by the results obtained on a physical phantom mimicking a pressure ulcer at an early stage. Computed elastograms showed strain differences between areas mimicking healthy and pathological tissues.

Compared to the results on numerical data, these elastograms showed a different strain pattern, which could be attributed to the different designs of the simulated and experimental phantoms. Indeed, for building procedure reasons, the area mimicking the pressure ulcer in the physical phantom is much wider than those in simulations and completely covers the bone. However, both numerical and experimental results demonstrate that US elastography can detect an abnormally stiff area corresponding to a deep pressure ulcer in development, even though no particular symptom is visible on the skin.

Finally, *in vivo* experiments were conducted on a rat model. A maintained pressure was applied on the animal thigh during 60 min, with a view to generate a pressure ulcer. It has been shown in a previous study,[14] based on histologies, that the protocol used in our experiment (in particular, the same compressing device and level of pressure were considered) leads to irreversible muscle cell death after only 15 min of exposition. The same paper concludes that changes in mechanical properties follow morphological damages and cellular death. RF US data, acquired before and after application of this pressure, were processed with our strain estimator. Elastograms revealed a difference in the way tissues behaved before and after the pressure was applied, which strongly suggest the presence of a pathological area.

These first results naturally require confirmation by performing many other *in vivo* experiments. In particular, acquisitions on human patients can be envisaged using lower frequency probe to image a larger area of tissue.

Nevertheless, these first experiments demonstrate that US elastography is a promising technique for pressure ulcer detection, especially at an early stage of the pathology, when the disease is still visually undetectable. In the absence of any other technique, this is also a first step toward the development of an objective and reliable tool.

a)Electronic mail: jean-francois.deprez@eng.ox.ac.uk

[1]National Pressure Ulcer Advisory Panel, "Pressure ulcers in America: Prevalence, incidence, and implications for the future. An executive summary of the National Pressure Ulcer Advisory Panel monograph," Adv. Skin Wound Care **14**(4), 208–215 (2001).

[2]K. O'Dea, "Prevalence of pressure damage in hospital patients in the UK," J. Wound Care **2**, 221–225 (1993).

[3]S. E. Sedory Holzer, A. Camerota, L. Martens, T. Cuerdon, J. Crystal-Peters, and M. Zagari, "Costs and duration of care for lower extremity ulcers in patients with diabetes," Clin. Ther. **20**(1), 169–181 (1998).

[4]H. Miller and J. Delozier, "Cost implications of the pressure ulcer treatment guideline," Columbia, MD, Center for Health Policy Studies, 1994:17, Contract 2282-91-0070 (1994).

[5]I. Cho and M. Noh, "Braden scale: Evaluation of clinical usefulness in an intensive care unit," J. Adv. Nurs. **66**(2), 293–302 (2010).

[6]R. J. Goldman and R. Salcido, "More than one way to measure a wound: An overview of tools and techniques," Adv. Skin Wound Care **15**, 236–243 (2002).

[7]A. A. Weber, C. Gehin, G. Moddy, J. Jossinet, and E. T. McAdams, "Characterization of a multi-frequency wound impedance mapping instrument," Proceedings of the 30th IEEE EMBS Conference, Vancouver, Canada, 20–24 August, 2008.

[8]S. Treuillet, B. Albouy, and Y. Lucas, "Three-dimensional assessment of skin wounds using standard digital camera," IEEE Trans. Med. Imaging **28**(5), 752–762 (2009).

[9]E. S. Andersen and T. Karlsmark, "Evaluation of four non-invasive methods for examination and characterization of pressure ulcers," Skin Res. Technol. **14**, 270–276 (2008).

[10]R. Meffre, C. Gehin, P. M. Schmitt, F. De Oliveira, and A. Dittmar, "New methodology for preventing pressure ulcers using actimetry and autonomous nervous system recording," Proceedings of the 28th IEEE EMBS Conference, New York, NY, 30 August–3 September 2006 (unpublished).

[11]R. K. Daniel, D. L. Priest, and D. C. Weatley, "Etiological factors in pressure sores: An experimental model," Arch. Phys. Med. Rehabil. **62**, 492–498 (1981).

[12]S. M. Dinsdale, "Decubitus ulcers: Role of pressure and friction in causation," Arch. Phys. Med. Rehabil. **55**, 147–152 (1974).

[13]M. Kosiak, "Etiology of decubitus ulcers," Arch. Phys. Med. Rehabil. **42**, 19–29 (1961).

[14]A. Gefen, N. Gefen, E. Linder-Ganz, and S. S. Margulies, "In vivo muscle stiffening under bone compression promotes deep pressure sores," J. Biomech. Eng. **127**, 512–524 (2005).

[15]E. Linder-Ganz and A. Gefen, "Stress analyses coupled with damage laws to determine biomechanical risk factors for deep tissue injury during sitting," J. Biomech. Eng. **131**(1), 011003 (2009).

[16]C. V. Bouten, C. W. Oomens, F. P. Baaijens, and D. L. Bader, "The etiology of pressure ulcer: Skin deep or muscle bound?," Arch. Phys. Med. Rehabil. **84**, 616–619 (2003).

[17]C. W. J. Oomens, S. Loerakker, and D. L. Bader, "The importance of internal strain as opposed to interface pressure in the prevention of pressure related deep tissue injury," J. Tissue Viability **19**(2), 35–42 (2010).

[18]T. A. Krouskop, D. R. Dougherty, and S. F. Levinson, "A pulsed Doppler ultrasonic system for making noninvasive measurements of the mechanical properties of soft tissue," J. Rehabil. Res. Dev. **24**, 1–8 (1987).

[19]J. Ophir, I. Céspedes, H. Ponnekanti, Y. Yazdi, and X. Li, "Elastography: A quantitative method for imaging the elasticity of biological tissues," Ultrason. Imaging **13**, 111–134 (1991).

[20]M. Tanter, J. Bercoff, A. Athanasiou, T. Deffieux, J. L. Gennisson, G. Montaldo, M. Muller, A. Tardivon, and M. Fink, "Quantitative assessment of breast lesion viscoelasticity: Initial clinical results using supersonic shear imaging," Ultrasound Med. Biol. **34**, 1373–1386 (2008).

[21]K. Konig, U. Scheipers, A. Pesavento, A. Lorenz, H. Ermert, and T. Senge, "Initial experiences with real-time elastography guided biopsies of the prostate," J. Urol. (Paris) **174**, 115–117 (2005).

[22]L. Sandrin, B. Fourquet, J. M. Hasquenoph, S. Yon, C. Fournier, F. Mal, C. Christidis, M. Ziol, B. Poulet, F. Kazemi, M. Beaugrand, and R. Palau, "Transient elastography: A new noninvasive for assessment of hepatic fibrosis," Ultrasound Med. Biol. **29**(12), 1705–1713 (2003).

[23]R. L. Maurice, J. Ohayon, Y. Frétigny, M. Bertrand, G. Soulez, and G. Cloutier, "Noninvasive vascular elastography: Theoretical framework," IEEE Trans. Med. Imaging **23**(2), 164–180 (2004).

[24]S. K. Alam, J. Ophir, and E. Konofagou, "An adaptive strain estimator for elastography," IEEE Trans. Ultrason. Ferroelectr. Freq. Control **45**, 461–472 (1998).

[25]E. Brusseau, C. Perrey, P. Delachartre, M. Vogt, D. Vray, and H. Ermert, "Axial strain imaging using a local estimation of the scaling factor from RF ultrasound signals," Ultrason. Imaging **22**(2), 95–107 (2000).

[26]E. Brusseau, J. Kybic, J. F. Deprez, and O. Basset, "2D locally regularized tissue strain estimation from radio-frequency ultrasound images: theoretical developments and results on experimental data," IEEE Trans.

Med. Imaging **27**(2), 145–160 (2008).

[27]A. P. Sarvazyan, O. V. Rudenko, S. D. Swanson, J. B. Fowlkes, and S. Y. Emelianov, "Shear wave elasticity imaging—A new ultrasonic technology of medical diagnostic," Ultrasound Med. Biol. **24**, 1419–1435 (1998).

[28]K. Nightingale, M. S. Soo, R. Nightingale, and G. Trahey, "Acoustic radiation force impulse imaging: In vivo demonstration of clinical feasibility," Ultrasound Med. Biol. **28**, 227–235 (2002).

[29]J. Bercoff, M. Tanter, and M. Fink, "Supersonic shear imaging: A new technique for soft tissue elasticity mapping," IEEE Trans. Ultrason. Ferroelectr. Freq. Control **51**(4), 396–409 (2004).

[30]J. F. Deprez, E. Brusseau, C. Schmitt, G. Cloutier, and O. Basset, "3D estimation of soft biological tissue deformation from radio-frequency ultrasound volume acquisitions," Med. Image Anal. **13**, 116–127 (2009).

[31]P. T. Boggs and J. W. Tolle, "Sequential quadratic programming," Acta Numerica **4**, 1–51 (1995).

[32]B. Barrois, L. Heitler, and P. Ribinik, *L'escarre: Les basiques* (Edition Asymptote, Paris, 1999).

[33]J. Y. Rho, R. B. Ashman, and C. H. Turner, "Young's modulus of trabecular and cortical bone material: Ultrasonic and microtensile measurements," J. Biomech. **26**(2), 111–119 (1993).

[34]B. K. Hoffmeister, S. R. Smith, S. M. Handley, and J. Y. Rho, "Anisotropy of Young's modulus of human tibial cortical bone," Med. Biol. Eng. Comput. **38**(3), 333–338 (2000).

[35]T. A. Krouskop, T. M. Wheeler, F. Kallel, B. S. Garra, and T. Hall, "Elastic moduli of breast and prostate tissues under compression," Ultrason. Imaging **20**, 260–274 (1998).

[36]J. Meunier and M. Bertrand, "Ultrasonic texture motion analysis: Theory and simulation," IEEE Trans. Med. Imaging **14**(2), 293–300 (1995).

[37]K. C. Chu and B. K. Rutt, "Polyvinyl alcohol cryogel: An ideal phantom material for MR studies of arterial flow and elasticty," Magn. Reson. Med. **37**(2), 314–319 (1997).

[38]J. Fromageau, E. Brusseau, D. Vray, G. Gimenez, and P. Delachartre, "Characterization of PVA cryogel for intravascular ultrasound elasticity imaging," IEEE Trans. Ultrason. Ferroelectr. Freq. Control **50**(10), 1318–1324 (2003).

[39]J. Fromageau, J. L. Genisson, C. Schmitt, R. L. Maurice, R. Mongrain, and G. Cloutier, "Estimation of polyvinyl alcohol cryogel mechanical properties with four ultrasound elastography methods and comparison with gold standard testings," IEEE Trans. Ultrason. Ferroelectr. Freq. Control **54**(3), 498–509 (2007).

[40]E. M. Landis, "Micro-injection studies of capillary blood pressure in human skin," Heart **15**, 209–228 (1930).

[41]D. L. Bader, "The recovery characteristics of soft tissues following repeated loading," J. Rehabil. Res. Dev. **27**, 141–150 (1990).

[42]M. A. Janvier, L. G. Durand, M. H. Roy Cardinal, I. Renaud, B. Chayer, P. Bigras, J. de Guise, G. Soulez, and G. Cloutier, "Performance evaluation of a medical robotic 3D-ultrasound imaging system," Med. Image Anal. **12**, 275–290 (2008).